



Effects of SO₂ on optical properties of secondary organic aerosol generated from photooxidation of toluene under different relative humidity

Wenyu Zhang^{1,2}, Weigang Wang^{*1,2}, Junling Li^{1,2}, Chao Peng^{1,2}, Kun Li⁴, Li Zhou⁵, Bo Shi^{1,2}, Yan Chen^{1,2}, Mingyuan Liu^{1,2}, and Maofa Ge^{*,1,2,3}

¹ State Key Laboratory for Structural Chemistry of Unstable and Stable Species, Beijing National Laboratory for Molecular Sciences (BNLMS), CAS Research/Education Center for Excellence in Molecular Sciences, Institute of Chemistry, Chinese Academy of Sciences, Beijing 100190, PR China

² University of Chinese Academy of Sciences, Beijing 100049, P. R. China

³ Center for Excellence in Regional Atmospheric Environment, Institute of Urban Environment, Chinese Academy of Sciences, Xiamen 361021, PR China

⁴ Air Quality Research Division, Environment and Climate Change Canada, Toronto, Ontario M3H 5T4, Canada

⁵ College of Architecture and Environment, Sichuan University, Chengdu, China

* E-mail addresses: W. Wang (wangwg@iccas.ac.cn) and M. Ge (gemaofa@iccas.ac.cn)



Abstract. Secondary organic aerosol (SOA) have great impacts on air quality, climate change and human health. The composition and physicochemical properties of SOA differ a lot for they originated under different atmospheric conditions and from various precursors and oxidations. In this work, photooxidation experiments of toluene were performed under four conditions (dry, dry with SO₂, wet, 5 and wet with SO₂) to investigate the effect of SO₂ under different relative humidity on the composition and optical properties of SOA at the wavelength of 375 nm and 532 nm. According to our results, the increase of humidity enhances not only light absorption, but also scattering property of SOA. Highly conjugated oligomers formed through multiphase reaction might be the reasons of this phenomenon. Adding SO₂ slightly lower the real part of complex refractive index (n) of SOA: $n_{\text{dry, SO}_2} < n_{\text{dry}}, n_{\text{wet, SO}_2} <$ 10 n_{wet} , which might be a result of the partitioning of low oxidation state products, such as alcohols, esters, and so on. The imaginary part of complex refractive index (k) are enhanced under condition dry with SO₂ compared to condition dry might because of the enhancement of charge transfer complexes, a great contributor to ultraviolet and visible light absorption. Condition wet with SO₂ shows the combined effect of SO₂ and humidity condition. The extinction properties of toluene-derived SOA under condition wet 15 and SO₂ are increased about 30% compared to condition dry. Our results suggest that various atmospheric conditions will affect the composition and optical properties of SOA, which have significant implications for evaluating the impacts of SOA on the rapid-formation of regional haze, global radiative balance and climate change.

20

25

30



1. Introduction

Secondary organic aerosol (SOA) account for a major fraction of the atmospheric fine particulate matter ($PM_{2.5}$), and have significant impacts on air quality, climate change and human health (Seinfeld and Pandis, 2006; Jimenez et al., 2009; Hallquist et al., 2009; Huang et al., 2014). Globally, SOA could influence the radiative balance by scattering and absorbing solar and terrestrial radiation directly, and by impacting cloud formation and their lifetimes indirectly (IPCC, 2013; Andreae and Gelencser, 2006; Moise et al., 2015). On the urban and regional scale, SOA contribute to the degradation of visibility and adversely influence human health (Watson, 2002; Pope et al., 2002). Quantifying optical properties of SOA is one of the key problems of accessing anthropogenic pollution for visibility, air quality, and climate change, and also one of the most urgent issues in the atmospheric sciences (Laskin et al., 2015; Moise et al., 2015; Andreae and Gelencser, 2006).

Aromatic compounds, accounting for 20% - 40% v/v of gasoline fuel, are one of the representative anthropogenic VOCs, and play an important role in the formation of tropospheric ozone and SOA (Odum, 1997; Ng et al., 2007; Zhang et al., 2015; Odum et al., 1997). Among these aromatic hydrocarbons, toluene is thought to be one of the most important SOA precursors, because of its strong emissions and SOA formation potential (Hildebrandt et al., 2009; Odum et al., 1997; Odum et al., 1996; Tao et al., 2017). The optical properties of aromatics derived SOA has received significant attention over the last decade, most of them were focused the effect of NO_x on optical properties of aromatics SOA (Li et al., 2014; Kim and Paulson, 2013; Lin et al., 2015; Nakayama et al., 2013). In particular, Li et al studied the effects of multiphase processes on the optical properties of m-xylene SOA (Li et al., 2017c). However, the optical properties of toluene-derived SOA under various atmospheric relevant conditions remain unclear, which limit our understanding of the severe and complex air pollution.

Recent studies have shown that SOA is a dominant fraction of the total atmospheric aerosol burden, particularly in heavy-polluted areas (Guo et al., 2014; Tao et al., 2017). Field experiments reported that the atmospheric concentration of SO_2 could be up to nearly 200 ppb in heavy haze pollution episodes in China, while the formation and growth rates of SOA and sulphate, which significantly contribute to severe haze pollution, were much faster than the rates in clean periods (Li et al., 2017a). Previous studies mostly focused on the enhancement of SOA yields introduced by the presence of SO_2 for isoprene, α -pinene and anthropogenic precursors (Santiago et al., 2012; Kleindienst et al., 2006; Liggio and Li, 2013). They also revealed that SOA yields enhancing effect is due to the fact that the acidic aerosol products of SO_2 and the formation of new particles. Surratt et al found that reactions of epoxydiols of isoprene in the presence of acidic aerosol produced from the oxidation of SO_2 could be a substantial source of "missing urban SOA" (Surratt et al., 2010). M. Jaoui showed that the addition of SO_2 would make the color of SOA generated from photooxidation of α -pinene together with toluene darker and browner, oligomers and nitrogeneous organic compounds were detected in the SOA extracts (Jaoui et al., 2008). Nakayama et al investigated the effect of SO_2 on optical properties of isoprene under various NO_x concentrations and oxidation pathways (Nakayama et al., 2015; Nakayama et al., 2018). However, more researches are need for the role of SO_2 in the subsequent optical properties of SOA formed from various VOCs.



Field studies have shown that haze events were often accompanied with high relative humidity (RH) (Sun et al., 2016a; Sun et al., 2016b), and organic aerosols were mostly liquid (Shiraiwa et al., 2017; Liu et al., 2017). Multiphase reactions take an important place in SOA formation as well, as shown in previous studies. For example, Jia et al (Jia and Xu, 2018) have shown that the yield of toluene SOA almost
5 doubled at relative humidity of 85 % compared to dry conditions (Hinks et al., 2018). Li et al found multiphase reactions would enhance light scattering and radiative forcing of m-xylene SOA (Li et al., 2017c). The impact of complicated air conditions on SOA generation, especially the effect of polluting gases (e.g., SO₂) and phase state, are in dire need for the forecasting, assessing, and controlling of the air pollution.

10 In this work, we investigated the effects of SO₂ on optical properties and chemical composition of SOA derived from toluene under different humidity. The results will greatly help the evaluation of toluene derived SOA on atmospheric visibility and climate change under complicated pollution conditions. More importantly, the data in current study will be highly useful for the simulation of models and field observations performed at various pollution conditions.

15 2. Methods

2.1 Smog chamber experiments and online measurements

Experiments were performed in a 5 m³ dual-reactor smog chamber, the details of which were described elsewhere (Wang et al., 2015; Li et al., 2017c; Li et al., 2017b). Briefly, the reactors were placed in a thermally isolated enclosure, while temperature and RH can be well controlled by blowers and air
20 conditioner. The variation range of temperature was 0.5 °C and the limits for variability of RH was below 5%. Experiments were performed using multiple UV light sources, which result in a similar spectrum with solar radiation (Wang et al., 2015). During the experiments, the concentrations of NO, NO₂ and SO₂ were measured by corresponding gas analyzers (Teledyne API T200UP, and Thermo 48i). The concentration of toluene was measured by a proton transfer reaction quadrupole mass spectrometry
25 in H₃O⁺ mode (PTR-QMS, Ionicon). The size distributions, number concentrations and mass concentrations of SOA were determined by a scanning mobility particle sizer (SMPS), which was consisted of electrostatic classifier (EC, TSI 3080), differential mobility analyzer (DMA, TSI 3081) and condensation particle counter (CPC, TSI 3776). A density of 1.4 g cm⁻³ for toluene SOA was used according to the previous studies (Ng et al., 2007; Li et al., 2014).

30 The extinction coefficients at 532 nm were detected with a custom-built cavity ring-down spectrometers (CRDS), the details of which were given previously (Wang et al., 2012; Li et al., 2014; Li et al., 2017b). The scattering, absorption, and extinction coefficients at 375 nm were measured by a photoacoustic extinctions (PAX-375, Droplet Measurement Technologies).



2.2 Experimental conditions and off-line measurements

As shown in Table 1, four sets of experiments were conducted: D for dry condition ($RH < 5\%$, $SO_2 < 1$ ppb); DS for dry condition with SO_2 ($RH < 5\%$, $SO_2 = 30-50$ ppb); W for wet condition ($RH > 80\%$, $SO_2 < 1$ ppb); and WS for wet condition with SO_2 ($RH > 80\%$, $SO_2 = 30-50$ ppb). To ensure the results were reproducible, each kind of experiment was performed twice. Before each experiment, the chamber was flushed at least three times using zero air (AADCO 737-15), with the number concentration of particles lower than 50 cm^{-3} , and the concentrations of NO_x and SO_2 lower than 1 ppb. After preparation, a known volume of organic precursor was added to the chamber by a glass U-tube through zero air. HONO was then added into the chamber by bubbling a small flow of zero air through the immediately mixed solution of 1 mL of 1 wt% $NaNO_2$ and 2 mL of 10 wt% H_2SO_4 . The by-products NO and NO_2 were also introduced into the chamber. The concentration of toluene in the chamber was about 180 ppb, while total NO_x level was about 500 ppb. SO_2 was introduced into the chamber from a 29.6 ppm gas cylinder. For experiments under wet conditions, zero air was passed through a fuel cell humidifier (FC - 200 - 780 - 7MP, Perma pure), and the RH was above 80% before experiments started. The contents in the chamber were mixed for about 10 minutes, and then the UV lamps were turned on and photo-reaction started. When the SOA mass concentration stopped rising, lights were switched off and experiments stopped. All experiments were conducted at $25.0 \pm 0.5 \text{ }^\circ\text{C}$.

After each experiment, SOA were collected by PTFE filters ($0.2 \mu\text{m}$, 47mm, MILLIPORE FFLP), and then were extracted in 5 mL methanol in an ultrasonic bath for 30 minutes. The methanol solutions were analysed by an electrospray ionization time-of-flight mass spectrometry (ESI-TOF-MS) in positive and negative mode. A typical mass-resolving power of > 30000 was achieved at m/z 200, with an absolute mass error below 3 ppm. Each sample extract was measured in triplicate with an injection volume of 10 μL . The ions detected in filter blank were subtracted and molecular formulas in the samples were assigned to all ions with signal-to-noise ratios of greater than 10. The settings for ESI positive method was: capillary voltage 3 kV, nebulizer gas pressure 0.4 bar, dry gas flow rate 3 litres per minute, dry gas temperature $180 \text{ }^\circ\text{C}$, and mass detection range 100 - 1000. As for negative mode, capillary voltage was set to 2.5 kV, nebulizer gas pressure was 0.3 bar, dry gas flow rate was 4 litres per minute, dry gas temperature was $150 \text{ }^\circ\text{C}$, and mass detection was ranged from 200 to 1000.

The following chemicals were used without further purification: toluene ($\geq 99.5\%$) [Aladdin], sulphuric acid ($\geq 95\%$) [Beijing Chemical Works], sodium nitrite (98%) [Alfa Aesar], methanol (99.9%) [Fisher Chemical], SO_2 ($29.6 \times 10^{-6} \text{ mol/mol}$) [National Institute of Metrology].

2.3 Calculation of the complex refractive index

Complex refractive index ($RI, m = n + ki$) are the only intrinsic optical property of particles, including both refractive index n and absorptive index k (Bohren and Huffman, 1983; Bond and Bergstrom, 2006). The RI calculation method used in this study has been applied and approved in previous studies (Li et al., 2014; Li et al., 2017b; Li et al., 2017c; Li et al., 2018b; Peng et al., 2018; Li et al., 2018a). Briefly, the extinction coefficients (α_{ext}) at 532 nm measured by CRDS and the scattering, absorption, and extinction



coefficients at 375 nm measured by PAX-375 were calculated on the basis of Mie theory. For monodispersed spherical particles, α_{ext} can be represented by:

$$\alpha_{ext} = N\sigma_{ext} = \frac{1}{4}N\pi D^2 Q_{ext} \quad (1)$$

where σ_{ext} is the extinction cross section; N is the number concentration of particles; D is the diameter of particles, and Q_{ext} represents the extinction efficiency, which is the ratio of extinction cross section to the geometric area of the particles.

For polydispersed particles with a log-normal size distribution, and the geometric standard deviation (σ_g) smaller than 1.5, α_{ext} can be expressed to:

$$\alpha_{ext} = \frac{1}{4}S_{tot} Q_{ext} \quad (2)$$

where S_{tot} is the total surface concentration. A hypothesis was made for simplifying data processing, that Q_{ext} value of the polydispersed particles in the whole size distribution range was the same as Q_{ext} value of particles with the surface mean diameter (D_{sm}). The S_{tot} and D_{sm} was given by SMPS directly, of which the uncertainties are $\pm 1\%$ and $\pm 5\%$, respectively.

The value of Q_{ext} of particles with a given D_{sm} can be calculated through the Mie program subsequently. The best-fit complex index is determined by minimizing the following reduced merit function (χ_r):

$$\chi_r = \frac{1}{N} \sum_{i=1}^N (Q_{ext,measured} - Q_{ext,calculated}(n, k))_i^2 \quad (3)$$

2.4 Calculation of RI of products

RI of products are calculated by quantitative structure-property relationship, developed by Redmond and Thomson (Redmond and Thompson, 2011). In brief, the RI values are estimated by polarizability (α), degree of unsaturation (μ), mass density (ρ_m) and molecular weight (M) in Eq (4).

$$RI_{predicted} = 0.031717(\mu) + 0.0006087(\alpha) - 3.0227\left(\frac{\rho_m}{M}\right) + 1.38708 \quad (4)$$

The mass density of each molecule is estimated by the AIM model, which had high accuracy for 166 organic compounds (Girolami, 1994). One thing needs to be noticed is that the model should be used at 550 nm. It would cause acceptable small errors for using it at 532 nm. This method was employed in our previous as well (Li et al., 2017b; Li et al., 2018b; Li et al., 2017c; Peng et al., 2018).

3. Results and discussion

3.1 General results of experiments

As shown in Figure 1, particles were generated only several minutes after the lamps turned on. Although the concentrations of NO differed in different conditions, the max concentrations of NO_x were about the same, ~500 ppb. The consumptions of the organic precursor were similar in all experiments (~100 ppb), indicating the similar OH exposures and oxidation levels. At the end of the experiments, the S_{tot} of particles were about 2.9×10^9 , 4.3×10^9 , 3.8×10^9 , 6.9×10^9 $nm^2 cm^{-3}$ in condition D, DS, W and WS,



respectively. The addition of SO₂ caused an enhancement of total surface concentrations of the particles, probably because of the formation of new particles and/or acidic catalysed reactions, as implied in previous studies (Chu et al., 2016;Deng et al., 2017;Hallquist et al., 2009). Moreover, the S_{tot} under wet conditions were higher than that under dry conditions as well, probably due to aqueous reactions of water soluble products, as indicated previously (Jia and Xu, 2018;Kamens et al., 2011;Hinks et al., 2018).

5 The extinction efficiencies of SOA under four different conditions at 375 nm and 532 nm are illustrated in Figure 2. The fitting curves match well with experiment data points under each condition. At 532 nm, the average values of RI are 1.412, 1.348, 1.504 and 1.468 under condition D, DS, W and WS, respectively. The complex refractive indexes at 375 nm under condition D, DS, W and WS are 1.45, 1.37+0.014i, 1.4566+0.022i and 1.51+0.012i. The refractory indexes of the SOA as a function of surface mean diameter (D_{sm}) under various conditions are shown in Figure S1. As the reaction proceeded, surface mean diameter of particles increased while n decreased. This phenomenon was observed in all experiments in this study and agreed well with previous studies (Li et al., 2014;Li et al., 2017b;Peng et al., 2018).

10

15 The refractory indexes under dry conditions (Figure 2 (a) and Figure 3 (a)) are comparable with previous studies (Nakayama et al., 2013;Kim and Paulson, 2013;Li et al., 2014;Moise et al., 2015). For example, Kim et al (Kim et al., 2010;Kim and Paulson, 2013) discovered that the values of RI of toluene-derived SOA at 532 nm were in the range of 1.35 to 1.61 (experiment conditions: 3.2 ppm toluene, and 3.1 ppm NO_x). Li et al found RI of toluene SOA was about 1.5 under HONO condition, and the concentration of

20 NO_x was about 1 ppm. The slightly lower n in current study (1.412) might be a result of the lower NO_x level, as Nakayama et al found that higher NO_x level would lead to higher n (Nakayama et al., 2013). As shown in Figure 3, n and imaginary part of RI (k) at 532 nm and 375 nm under four different conditions differ greatly. At 375 nm, k under condition W is the highest, while k under condition DS and WS are the second highest, about 0.014. For n, the highest value appears in condition W, while the lowest shows in condition DS. All values of n at 375 nm were larger than those at 532 nm with difference of 0.022 - 0.062. Real and imaginary part of RI increase as wavelength decreasing, which were in good accordance with previous studies (Moise et al., 2015;Flores et al., 2014a;Flores et al., 2014b;Lin et al., 2015;Liu et al., 2016a;Liu et al., 2015;Nakayama et al., 2013;Nakayama et al., 2018;Nakayama et al., 2015). For example, Liu et al (Liu et al., 2015) found the values of RRI of toluene-derived secondary

25 organic material reduced about 0.1 with wavelength changing from 240nm to 800nm. In this case, the optical properties of secondary organic aerosol should be concerned differently at different wavelength, particularly in UV-vis band.

30 To explain the RI variations of toluene-derived SOA under different conditions, aerosols were collected and analysed by ESI-TOF-MS both in positive and negative mode. Mass spectrometry have enabled molecular characterisation of organic macromolecules in SOAs by their high resolution and mass accuracy (Lin et al., 2014;Lin et al., 2012;Hinks et al., 2018). Products are inferred based on mass spectra (MS) and previous studies (Kelly et al., 2010;Hinks et al., 2018;Liu et al., 2016c;Nakayama et al., 2015). Most products are concentrated around 200-400 m/z (Figure 4 and S2, Table 2, S1 and S2), and some of them containing organonitrogen group, which could be seen more clearly in negative mode. However,

40 previous studies mainly focused on lower mass range (< 200 Da) (Hinks et al., 2018;Forstner et al.,



1997;Staudt et al., 2014;Wang et al., 2018;Birdsall et al., 2010), e.g., Birdsall et al. (Birdsall et al., 2010) detected benzaldehyde, cresol, phenol, and butenedial in the photooxidation process of toluene, under both low-NO_x and high-NO_x conditions. In this work, we tried to analyse the *m/z* between 200 and 400 and discussed the effect of SO₂ under different humidity. The representative identified molecular weight, 5 molecular formula, and calculated RI values of toluene SOA are shown in Figure 5 and Table 2. More details are given in Table S1 and Table S2.

3.2 Effects of high humidity

High relative humidity brings substantial increase to RI values for toluene-derived SOA (Figure 2 and Figure 3). Refractory indexes rise from 1.45 to 1.566 at 375 nm and 1.412 to 1.504 at 532 nm in absence 10 of SO₂. Previous studies reported the similar findings, e.g., Li et al (Li et al., 2017c) found that high RH would enhance the light scattering of SOA by multiphase reactions; Liu et al (Liu et al., 2016a) discovered that mass absorption coefficient values at 365nm of SOA produced by photooxidation of trimethylbenzene and toluene were enhanced when reaction RH increased from <5% to 80%.

Wet conditions would lead to higher RI values compared with dry condition, and bring about the 15 formation of macromolecular polymers, which could be seen in Figure 5. Macromolecular oligomers above 500 Da appear high relative intensities under wet conditions, and these products possess high RI values, as shown in Table 2, S1 and S2 likewise. Multiphase reactions in the presence of liquid water lead to the formation of oligomers from intermediate products such as glyoxal and methylglyoxal, resulting in large enhancement in RI, which was proved in previous studies (Li et al., 2017c;Liu et al., 2016a).

Highly conjugated oligomers produced from multiphase reactions such as acid-catalyzed aldol 20 condensations are found in MS under condition W, especially in positive mode, which could extend light absorption to longer wavelengths (Lambe et al., 2013). Lambe et al found that the conjugated double bonds could enhance the absorption in the UV-Vis light as well (Lambe et al., 2013). This phenomenon also is approved in previous reports (Jia and Xu, 2018;Faust et al., 2017;Liu et al., 25 2018b).

3.3 Effects of SO₂ under dry condition

It was shown in Figure 2 and 3 that adding SO₂ resulted in the decrease of refractory indexes of toluene-derived SOA from 1.45 to 1.37 at 375 nm and from 1.412 to 1.348 at 532 nm under dry 30 conditions. Compared with condition D, *k* under condition DS increased 0.014. Similar phenomenon was also found in other systems, e.g., Nakayama et al (Nakayama et al., 2015) discovered that adding SO₂ caused refractory indexes of isoprene-derived SOA decreased, while the imaginary part increased. Nakayama et al (Nakayama et al., 2018) further found that that adding SO₂ would cause significant light absorption at short visible and ultraviolet wavelengths of isoprene-derived SOA under OH oxidation progresses, which was quite similar with our results.

To clearly see the change of chemical compositions under condition D and DS, the subtraction plots of 35 mass spectra are shown in Figure S2. As we can see in Figure S2 (a), adding SO₂ would cause the relative intensities of products increase with lower molecular weight (< 200 Da). These products are mainly



alcohols and esters with smaller molecular weight, such as butanehexol, cyclohexanepentol, and methylpentitol, n of which are lower than 1.4. The reason of this occasion probably is the addition of SO_2 would cause large amounts of new particles formation and high particle number concentrations in the system (Chu et al., 2015; Chu et al., 2016; Deng et al., 2017; Liu et al., 2018a), and this could provide
5 larger aerosol surface area and adsorb high-volatile small molecules into the particle phase (Li et al., 2018b). These small molecules products usually possessed high volatility and low oxidation state, which would also reduce the oxidation state of aerosols generated by toluene. Previous studies had found similar phenomenon, for example, Zhao et al (Zhao et al., 2018) found that high SO_2 would decrease the ratio O/C whether in α -pinene or limonene system, while Liu et al (Liu et al., 2016b) discovered that the
10 oxidation state of carbon (OS_c) were -0.51 ± 0.06 for SOA formed from light-duty gasoline vehicles (LDGV) exhaust with SO_2 and -0.19 ± 0.08 without SO_2 , which all implied that adding SO_2 would reduce the oxidation state of SOA. One thing should be noticed was that our off-line analytical method would cause the loss of a large part of alcohols and esters with small molecular weight, which might overestimate the values of RIs.

15 Charge transfer (CT) complexes are a significant source of brown carbon (BrC) (Phillips and Smith, 2014), which are formed from weak associations between molecules or separate parts of a single molecule, could give rise to electronic transitions in the UV–visible spectrum. CT complexes lead to optical transitions through a transfer of charge from a donor group, such as hydroxyl to an acceptor group, such as a ketone or aldehyde. The concentrations of small molecular weight alcohols are higher
20 under condition DS compared to condition D in aerosol phase. These SOA products under condition DS might comprise CT complexes thus present absorption at 375 nm. Another reason of the increase of k at 375 nm is the formation of unsaturated oligomers through dehydration reactions during photooxidation in the presence of SO_2 , as suggested by Nakayama (Nakayama et al., 2015; Nakayama et al., 2018). As for organosulfate, another kind of BrC, we didn't detect them in condition DS, which
25 is in coincidence with previous studies (Nakayama et al., 2015; Nakayama et al., 2018; Staudt et al., 2014).

3.4 Effects of SO_2 under wet condition

In wet condition with SO_2 , the average refractory index of toluene SOA are 1.51 at 375 nm and 1.468 at 532 nm, higher than condition DS and lower than condition W (Figure 2 and 3). As for absorption, k
30 under condition WS are lower than condition W, and similar to condition DS. Figure 4 shows the subtraction plots of MS between condition DS or W and WS. Low oxidation organic matters and macromolecular oligomers are both found in the MS. Under WS condition, macromolecular oligomers are in high-concentration compared to dry condition with SO_2 , while low organic matters are in large proportion compared to wet condition without SO_2 . Under this combined effects, the values of
35 refractory indexes of SOA are lower than condition W and higher than condition DS. The k under condition WS are almost equal to those under condition DS, while lower than the values under condition W. Lower oxidation state and less conjugated oligomers caused by SO_2 might be the reason of this phenomenon, as proved in previous studies (Nakayama et al., 2015; Liu et al., 2016a).



The concentration of donor groups is lower than condition DS, resulting in lower concentration of CT complexes, which might another reason of reduce of k . The nitro-aromatic compounds are not found under condition WS. The combined effects of SO_2 and wet condition on optical properties of toluene SOA are first described to the best of our knowledge, which possesses significant influence on light absorption, extinction, visibility and direct radiative forcing of regional air, especially in complex polluted area. Our results provide some explanations for the observed variation, and further research is needed to quantify this synergetic effect.

4. Atmospheric and Climate Implication

The values of mass cross section (MAC) are calculated for conditions DS, W, WS at 375 nm, while method are described in Supporting Information. SOA under conditions D is not calculated because they appeared no absorption. The average values of MAC are 0.2749, 0.3082 and 0.2131 g/m^2 under condition DS, W and WS, respectively. These results are similar with Liu's work that wet condition would cause higher values of MAC than dry condition (Liu et al., 2016a). However, MAC values in Liu's work are about 0.4 g/m^2 at wet conditions and 0.01 g/m^2 at dry conditions at 380 nm, higher than our results, which is likely due to the high concentration of OH in their study.

The impacts of atmospheric and climate are assessed by comparing the ratio of light extinction efficiency and simple forcing efficiency (SFE) under four different conditions, while the results are shown in Figure 6 and S3. Aerosol sizes between 100nm and 250 nm were circled because these were atmospherically relevant sizes of aerosols (Zhang et al., 2015; Tao et al., 2017). As shown in Figure 6, adding SO_2 would cause light extinction efficiency reduce about 16% -35% with average of 25% at 532 nm, and humid conditions would enhance light extinction efficiency about 36%-64% with average of 50%. As for the comprehensive impact made by SO_2 and high humidity, the light extinction efficiency would increase about 16% - 47% with average of 30%. This result confirms that SOA generated under complex pollution conditions might make a greater impact on the visibility reduction, the atmospheric photochemical reactions, and secondary species formation (Dickerson et al., 1997).

We estimate the clear-sky direct radiative forcing per unit optical depth with the help of the SFE concept, as mentioned in Supporting Information. Figure S3 shows the SFE of toluene-derived SOA under condition D, DS, W and WS at 375 nm and 532 nm, which could also reflect the change of direct radiative forcing (DRF). The forcing efficiency crosses over from negative (warming) to positive (cooling) values at diameter ≈ 200 nm under condition DS, W and WS. The lowest SFE values, about -35 W/g, are shown in condition W, while at diameter around 200 nm the SFE values are -10 and -20 W/g under condition WS and DS, respectively. All values of SFE at 532 nm are above zero, which means toluene SOA show cooling effects on climate change. SFE values of condition DS decreased about 25% compared to condition D, and the SFE of condition W and WS increased about 50% and 30%, which is similar with extinction efficiency. SFE values in our system are in coincidence with those of organic aerosols from wood combustion and burning of boreal peatlands (Chen and Bond, 2010; Chakrabarty et al., 2016). Our model doesn't include hygroscopicity and other factors, which would increase particle size and negative forcing. On this situation, our forcing is much lower than those in global climate



models (Schulz et al., 2006). A full climate model would be necessary to determine the actual forcing caused by this effects caused by SO₂ and humidity as well.

5. Conclusion

5 The effect of SO₂ under different humidity on optical properties of SOA photo-oxidized by toluene have
been investigated in this study. The results show that for the experimental system with RH greater than
80%, as expected, the increase in humidity greatly enhanced the RI of SOA, from 1.412 to 1.504 at
532nm and from 1.45 to 1.566+0.022i at 375 nm, which is probably because of the macromolecules
formation from multiphase reactions. Adding SO₂ can reduce refractory indexes of SOA at 375 nm and
532 nm whether under low or high humidity. RI values of toluene SOA produced under SO₂ and dry
10 condition are 1.37+0.014i at 375 nm and 1.348 at 532 nm, while RI values under dry and SO₂-free
conditions are 1.412 at 532 nm and 1.45 at 375 nm. The reasons of this phenomenon might be that adding
SO₂ would cause large amounts of new particles formation and high particle surface concentrations in the
system, which could adsorb higher volatile molecules into the particle phase. Higher volatile molecules
produce lower oxidation state and lower n values, resulting in the decrease of n of toluene SOA. The
15 increase in k is probably related to the enhancement of CT complexes and dehydration reactions on
acidic particles. For the experimental system under sulfur dioxide and high humidity condition, the
refractory indexes were higher than SOA derived from conditions without SO₂ and low humidity. The
imaginary indexes under this condition are lower than wet condition without SO₂ for less conjugated
oligomers formed. The extinction properties under condition WS are about 30% higher than condition D.
20 The results here highlighted that combined effect of SO₂ and high humidity which could greatly enhance
the refractive index, light scattering, and direct radiative forcing of toluene SOA and potentially others.
These results will improve our understanding of SOA optical properties, especially under complex
atmospheric conditions.

25

Author contributions. WW, MG and WZ conceived and led the studies. WZ, JL and CP performed chamber simulation and data analysis. KL, LZ, BS, YC and ML discussed the results and commented on the manuscript. WZ prepared the manuscript with contributions from all co-authors.

30 Acknowledgements

This project was supported by The National Key Research and Development Program of China (2016YFC0202704), National research program for key issues in air pollution control (DQGG-0103) and the National Natural Science Foundation of China (91544227, 91844301, 41822703).

35



Reference

- Andreae, M. O., and Gelencser, A.: Black carbon or brown carbon? The nature of light-absorbing carbonaceous aerosols, *Atmos. Chem. Phys.*, 6, 3131-3148, <https://doi.org/10.5194/acp-6-3131-2006>, 2006.
- 5 Birdsall, A. W., Andreoni, J. F., and Elrod, M. J.: Investigation of the Role of Bicyclic Peroxy Radicals in the Oxidation Mechanism of Toluene, *J. Phys. Chem. A*20101143910655-10663, <https://doi.org/10.1021/jp105467e>, 2010.
- Bohren, C. F., and Huffman, D. R.: Absorption and scattering of light by small particles, John Wiley & Sons, Hoboken, NJ, 1983.
- 10 Bond, T. C., and Bergstrom, R. W.: Light Absorption by Carbonaceous Particles: An Investigative Review, *Aerosol Sci. Tech.*, 40, 27-67, <https://doi.org/10.1080/02786820500421521>, 2006.
- Chakrabarty, R. K., Gyawali, M., Yatavelli, R. L. N., Pandey, A., Watts, A. C., Knue, J., Chen, L.-W. A., Pattison, R. R., Tsiabart, A., Samburova, V., and Moosmüller, H.: Brown carbon aerosols from burning of boreal peatlands: microphysical properties, emission factors, and implications for direct radiative forcing, *Atmos. Chem. Phys.*, 16, 3033-3040, <https://doi.org/10.5194/acp-16-3033-2016>, 2016.
- 15 Chen, Y., and Bond, T. C.: Light absorption by organic carbon from wood combustion, *Atmos. Chem. Phys.*, 10, 1773-1787, <https://doi.org/10.5194/acp-10-1773-2010>, 2010.
- Chu, B., Liu, T., Zhang, X., Liu, Y., Ma, Q., Ma, J., He, H., Wang, X., Li, J., and Hao, J.: Secondary aerosol formation and oxidation capacity in photooxidation in the presence of Al₂O₃ seed particles and SO₂, *Sci. China. Chem.*, 58, 1426-1434, <https://doi.org/10.1007/s11426-015-5456-0>, 2015.
- 20 Chu, B., Zhang, X., Liu, Y., He, H., Sun, Y., Jiang, J., Li, J., and Hao, J.: Synergetic formation of secondary inorganic and organic aerosol: effect of SO₂ and NH₃ on particle formation and growth, *Atmos. Chem. Phys.*, 16, 14219-14230, <https://doi.org/10.5194/acp-16-14219-2016>, 2016.
- 25 Deng, W., Liu, T., Zhang, Y., Situ, S., Hu, Q., He, Q., Zhang, Z., Lü, S., Bi, X., Wang, X., Boreave, A., George, C., Ding, X., and Wang, X.: Secondary organic aerosol formation from photo-oxidation of toluene with NO_x and SO₂: Chamber simulation with purified air versus urban ambient air as matrix, *Atmos. Environ.*, 150, 67-76, <https://doi.org/10.1016/j.atmosenv.2016.11.047>, 2017.
- 30 Dickerson, R., Kondragunta, S., Stenchikov, G., Civerolo, K., Doddridge, B., and Holben, B.: The impact of aerosols on solar ultraviolet radiation and photochemical smog, *Science*, 278, 827-830, [10.1126/science.278.5339.827](https://doi.org/10.1126/science.278.5339.827), 1997.
- Faust, J. A., Wong, J. P., Lee, A. K., and Abbatt, J. P.: Role of Aerosol Liquid Water in Secondary Organic Aerosol Formation from Volatile Organic Compounds, *Environ. Sci. Technol.*, 51, 3, 1405-1413, <https://doi.org/10.1021/acs.est.6b04700>, 2017.
- 35 Flores, J. M., Washenfelder, R. A., Adler, G., Lee, H. J., Segev, L., Laskin, J., Laskin, A., Nizkorodov, S. A., Brown, S. S., and Rudich, Y.: Complex refractive indices in the near-ultraviolet spectral region



- of biogenic secondary organic aerosol aged with ammonia, *Phys. Chem. Chem. Phys.*, 2014, 16, 10629-10642, 10.1039/C4CP01009D, 2014a.
- Flores, J. M., Zhao, D. F., Segev, L., Schlag, P., Kiendler-Scharr, A., Fuchs, H., Watne, Å. K., Bluvshstein, N., Mentel, T. F., Hallquist, M., and Rudich, Y.: Evolution of the complex refractive index
5 in the UV spectral region in ageing secondary organic aerosol, *Atmos. Chem. Phys.*, 14, 5793-5806, <https://doi.org/10.5194/acp-14-5793-2014>, 2014
- Forstner, H. J. L., Flagan, R. C., and Seinfeld, J. H.: Secondary organic aerosol from the photooxidation of aromatic hydrocarbons: Molecular composition, *Environ. Sci. Technol.*, 3, 15, 1345-1358, <https://doi.org/10.1021/es9605376>, 1997.
- 10 Girolami, G. S.: A simple "back of the envelope" method for estimating the densities and molecular volumes of liquids and solids, *J. Chem. Educ.*, 1994, 71, 11, 962, <https://doi.org/10.1021/ed071p962>, 1994.
- Guo, S., Hu, M., Zamora, M. L., Peng, J., Shang, D., Zheng, J., Du, Z., Wu, Z., Shao, M., Zeng, L., Molina, M. J., and Zhang, R.: Elucidating severe urban haze formation in China, *Proc. Natl. Acad. Sci. U. S. A.*, 111, 17373-17378, <https://doi.org/10.1073/pnas.1419604111>, 2014.
- 15 Hallquist, M., Wenger, J. C., Baltensperger, U., Rudich, Y., Simpson, D., Claeys, M., Dommen, J., Donahue, N. M., George, C., Goldstein, A. H., Hamilton, J. F., Herrmann, H., Hoffmann, T., Iinuma, Y., Jang, M., Jenkin, M. E., Jimenez, J. L., Kiendler-Scharr, A., Maenhaut, W., McFiggans, G., Mentel, T. F., Monod, A., Prevot, A. S. H., Seinfeld, J. H., Surratt, J. D., Szmigielski, R., and Wildt, J.: The
20 formation, properties and impact of secondary organic aerosol: current and emerging issues, *Atmos. Chem. Phys.*, 9, 5155-5236, <https://doi.org/10.5194/acp-9-5155-2009>, 2009
- Hildebrandt, L., Donahue, N. M., and Pandis, S. N.: High formation of secondary organic aerosol from the photo-oxidation of toluene, *Atmos. Chem. Phys.*, 9, 2973-2986, <https://doi.org/10.5194/acp-9-2973-2009>, 2009
- 25 Hinks, M. L., Montoya-Aguilera, J., Ellison, L., Lin, P., Laskin, A., Laskin, J., Shiraiwa, M., Dabdub, D., and Nizkorodov, S. A.: Effect of relative humidity on the composition of secondary organic aerosol from the oxidation of toluene, *Atmos. Chem. Phys.*, 18, 1643-1652, <https://doi.org/10.5194/acp-18-1643-2018>, 2018
- Huang, R. J., Zhang, Y., Bozzetti, C., Ho, K. F., Cao, J. J., Han, Y., Daellenbach, K. R., Slowik, J. G.,
30 Platt, S. M., Canonaco, F., Zotter, P., Wolf, R., Pieber, S. M., Bruns, E. A., Crippa, M., Ciarelli, G., Piazzalunga, A., Schwikowski, M., Abbaszade, G., Schnelle-Kreis, J., Zimmermann, R., An, Z., Szidat, S., Baltensperger, U., El Haddad, I., and Prevot, A. S.: High secondary aerosol contribution to particulate pollution during haze events in China, *Nature*, 514, 218-222, 10.1038/nature13774, 2014.
- IPCC: Climate change 2013: the physical science basis: Working Group I contribution to the Fifth
35 assessment report of the Intergovernmental Panel on Climate Change, Cambridge University Press, 2013.



- Jaoui, M., Edney, E. O., Kleindienst, T. E., Lewandowski, M., Offenber, J. H., Surratt, J. D., and Seinfeld, J. H.: Formation of secondary organic aerosol from irradiated α -pinene/toluene/NO_x mixtures and the effect of isoprene and sulfur dioxide, *Journal of Geophysical Research*, 113, 10.1029/2007jd009426, 2008.
- 5 Jia, L., and Xu, Y.: Different roles of water in secondary organic aerosol formation from toluene and isoprene, *Atmos. Chem. Phys.*, 18, 8137-8154, <https://doi.org/10.5194/acp-18-8137-2018>, 2018
- Jimenez, J. L., Canagaratna, M. R., Donahue, N. M., Prevot, A. S. H., Zhang, Q., Kroll, J. H., DeCarlo, P. F., Allan, J. D., Coe, H., Ng, N. L., Aiken, A. C., Docherty, K. S., Ulbrich, I. M., Grieshop, A. P., Robinson, A. L., Duplissy, J., Smith, J. D., Wilson, K. R., Lanz, V. A., Hueglin, C., Sun, Y. L., Tian, J.,
10 Laaksonen, A., Raatikainen, T., Rautiainen, J., Vaattovaara, P., Ehn, M., Kulmala, M., Tomlinson, J. M., Collins, D. R., Cubison, M. J., Dunlea, E. J., Huffman, J. A., Onasch, T. B., Alfarra, M. R., Williams, P. I., Bower, K., Kondo, Y., Schneider, J., Drewnick, F., Borrmann, S., Weimer, S., Demerjian, K., Salcedo, D., Cottrell, L., Griffin, R., Takami, A., Miyoshi, T., Hatakeyama, S., Shimono, A., Sun, J. Y., Zhang, Y. M., Dzepina, K., Kimmel, J. R., Sueper, D., Jayne, J. T., Herndon, S. C., Trimborn, A. M., Williams, L. R., Wood, E. C., Middlebrook, A. M., Kolb, C. E., Baltensperger, U., and Worsnop, D. R.: Evolution of Organic Aerosols in the Atmosphere, *Science*, 326, 1525-1529,
15 10.1126/science.1180353, 2009.
- Kamens, R. M., Zhang, H., Chen, E. H., Zhou, Y., Parikh, H. M., Wilson, R. L., Galloway, K. E., and Rosen, E. P.: Secondary organic aerosol formation from toluene in an atmospheric hydrocarbon
20 mixture: Water and particle seed effects, *Atmos. Environ.*, 45, 2324-2334, <https://doi.org/10.1016/j.atmosenv.2010.11.007>, 2011.
- Kelly, J. L., Michelangeli, D. V., Makar, P. A., Hastie, D. R., Mozurkewich, M., and Auld, J.: Aerosol speciation and mass prediction from toluene oxidation under high NO_x conditions, *Atmos. Environ.*, 44, 361-369, <https://doi.org/10.1016/j.atmosenv.2009.10.035>, 2010.
- 25 Kim, H., Barkey, B., and Paulson, S. E.: Real refractive indices of α - and β -pinene and toluene secondary organic aerosols generated from ozonolysis and photo-oxidation, *J. Geophys. Res.: Atmos.*, 115, <https://doi.org/10.1029/2010jd014549>, 2010.
- Kim, H., and Paulson, S. E.: Real refractive indices and volatility of secondary organic aerosol generated from photooxidation and ozonolysis of limonene, α -pinene and toluene, *Atmos. Chem. Phys.*,
30 13, 7711-7723, <https://doi.org/10.5194/acp-13-7711-2013>, 2013.
- Kleindienst, T. E., Edney, E. O., Lewandowski, M., Offenber, J. H., and Jaoui, M.: Secondary organic carbon and aerosol yields from the irradiations of isoprene and α -pinene in the presence of NO_x and SO₂, *Environ. Sci. Technol.*, 40, 12, 3807-3812, <https://doi.org/10.1021/es052446r>, 2006.
- Lambe, A. T., Cappa, C. D., Massoli, P., Onasch, T. B., Forestieri, S. D., Martin, A. T., Cummings, M. J., Croasdale, D. R., Brune, W. H., Worsnop, D. R., and Davidovits, P.: Relationship between oxidation level and optical properties of secondary organic aerosol, *Environ. Sci. Technol.*, 47, 6349-6357,
35 <https://doi.org/10.1021/es401043j>, 2013.



- Laskin, A., Laskin, J., and Nizkorodov, S. A.: Chemistry of atmospheric brown carbon, *Chem. Rev.*, 115, 4335-4382, <https://doi.org/10.1021/cr5006167>, 2015.
- Li, H., Zhang, Q., Zhang, Q., Chen, C., Wang, L., Wei, Z., Zhou, S., Parworth, C., Zheng, B., Canonaco, F., Prévôt, A. S. H., Chen, P., Zhang, H., Wallington, T. J., and He, K.: Wintertime aerosol chemistry and haze evolution in an extremely polluted city of the North China Plain: significant contribution from coal and biomass combustion, *Atmos. Chem. and Phys.*, 17, 4751-4768, <https://doi.org/10.5194/acp-17-4751-2017>, 2017a.
- Li, J., Li, K., Wang, W., Wang, J., Peng, C., and Ge, M.: Optical properties of secondary organic aerosols derived from long-chain alkanes under various NO_x and seed conditions, *Sci. Total Environ.*, 10 579, 1699-1705, <https://doi.org/10.1016/j.scitotenv.2016.11.189>, 2017b.
- Li, J., Wang, W., Li, K., Zhang, W., Ge, M., and Peng, C.: Development and application of the multi-wavelength cavity ring-down aerosol extinction spectrometer, *J. Environ. Sci.*, 10.1016/j.jes.2018.04.030, 2018a.
- Li, K., Wang, W., Ge, M., Li, J., and Wang, D.: Optical properties of secondary organic aerosols generated by photooxidation of aromatic hydrocarbons, *Sci. Rep.*, 4, 4922, [10.1038/srep04922](https://doi.org/10.1038/srep04922), 2014.
- Li, K., Li, J., Liggio, J., Wang, W., Ge, M., Liu, Q., Guo, Y., Tong, S., Li, J., and Peng, C.: Enhanced light scattering of secondary organic aerosols by multiphase reactions, *Environmental science & technology*, 51, 3, 1285-1292, <https://doi.org/10.1021/acs.est.6b03229>, 2017c.
- Li, K., Li, J., Wang, W., Li, J., Peng, C., Wang, D., and Ge, M.: Effects of Gas-Particle Partitioning on Refractive Index and Chemical Composition of m-Xylene Secondary Organic Aerosol, *J. Phys. Chem. A.*, 122, 3250-3260, [10.1021/acs.jpca.7b12792](https://doi.org/10.1021/acs.jpca.7b12792), 2018b.
- Liggio, J., and Li, S. M.: A new source of oxygenated organic aerosol and oligomers, *Atmos. Chem. Phys.*, 13, 2989-3002, <https://doi.org/10.5194/acp-13-2989-2013>, 2013.
- Lin, P., Liu, J., Shilling, J. E., Kathmann, S. M., Laskin, J., and Laskin, A.: Molecular characterization of brown carbon (BrC) chromophores in secondary organic aerosol generated from photo-oxidation of toluene, *Phys. Chem. Chem. Phys.*, 17, 23312-23325, <https://doi.org/10.1039/c5cp02563j>, 2015.
- Lin, Y.-H., Zhang, Z., Docherty, K. S., Zhang, H., Budisulistiorini, S. H., Rubitschun, C. L., Shaw, S. L., Knipping, E. M., Edgerton, E. S., Kleindienst, T. E., Gold, A., and Surratt, J. D.: Isoprene Epoxydiols as Precursors to Secondary Organic Aerosol Formation: Acid-Catalyzed Reactive Uptake Studies with Authentic Compounds, *Environmental Science & Technology*, 46, 250-258, [10.1021/es202554c](https://doi.org/10.1021/es202554c), 2012.
- Lin, Y. H., Budisulistiorini, S. H., Chu, K., Siejack, R. A., Zhang, H., Riva, M., Zhang, Z., Gold, A., Kautzman, K. E., and Surratt, J. D.: Light-absorbing oligomer formation in secondary organic aerosol from reactive uptake of isoprene epoxydiols, *Environ Sci Technol*, 48, 12012-12021, [10.1021/es503142b](https://doi.org/10.1021/es503142b), 2014.



- Liu, C., Chen, T., Liu, Y., Liu, J., He, H., and Zhang, P.: Enhancement of Secondary Organic Aerosol Formation and its Oxidation State by SO₂ during Photooxidation of 2-Methoxyphenol, *Atmos. Chem. Phys.*, 19, 2687-2700, <https://doi.org/10.5194/acp-19-2687-2019>, 2019
- 5 Liu, J., Lin, P., Laskin, A., Laskin, J., Kathmann, S. M., Wise, M., Caylor, R., Imholt, F., Selimovic, V., and Shilling, J. E.: Optical properties and aging of light-absorbing secondary organic aerosol, *Atmos. Chem. Phys.*, 16, 12815-12827, <https://doi.org/10.5194/acp-16-12815-2016>, 2016a.
- Liu, P., Abdelmalki, N., Hung, H.-M., Wang, Y., Brune, W., and Martin, S.: Ultraviolet and visible complex refractive indices of secondary organic material produced by photooxidation of the aromatic compounds toluene and m-xylene, *Atmos. Chem. Phys.*, 15, 1435-1446, <https://doi.org/10.5194/acp-15-1435-2015>, 2015.
- 10 Liu, T., Wang, X., Hu, Q., Deng, W., Zhang, Y., Ding, X., Fu, X., Bernard, F., Zhang, Z., Lü S., He, Q., Bi, X., Chen, J., Sun, Y., Yu, J., Peng, P., Sheng, G., and Fu, J.: Formation of secondary aerosols from gasoline vehicle exhaust when mixing with SO₂, *Atmos. Chem. Phys.*, 16, 675-689, <https://doi.org/10.5194/acp-16-675-2016>, 2016b.
- 15 Liu, T., Wang, X., Hu, Q., Deng, W., Zhang, Y., Ding, X., Fu, X., Bernard, F., Zhang, Z., Lü S., He, Q., Bi, X., Chen, J., Sun, Y., Yu, J., Peng, P., Sheng, G., and Fu, J.: Formation of secondary aerosols from gasoline vehicle exhaust when mixing with SO₂, *Atmos. Chem. Phys.*, 16, 675-689, <https://doi.org/10.5194/acp-16-675-2016>, 2016c.
- Liu, T., Huang, D. D., Li, Z., Liu, Q., Chan, M., and Chan, C. K.: Comparison of secondary organic aerosol formation from toluene on initially wet and dry ammonium sulfate particles at moderate relative humidity, *Atmos. Chem. Phys.*, 18, 5677-5689, <https://doi.org/10.5194/acp-18-5677-2018>, 2018b.
- 20 Liu, Y., Wu, Z., Wang, Y., Xiao, Y., Gu, F., Zheng, J., Tan, T., Shang, D., Wu, Y., Zeng, L., Hu, M., Bateman, A. P., and Martin, S. T.: Submicrometer Particles Are in the Liquid State during Heavy Haze Episodes in the Urban Atmosphere of Beijing, China, *Environ. Sci. Technol. Lett.*, 4, 10, 427-432, <https://doi.org/10.1021/acs.estlett.7b00352>, 2017.
- Moise, T., Flores, J. M., and Rudich, Y.: Optical properties of secondary organic aerosols and their changes by chemical processes, *Chem. Rev.*, 115, 4400-4439, <https://doi.org/10.1021/cr5005259>, 2015.
- 25 Nakayama, T., Sato, K., Matsumi, Y., Imamura, T., Yamazaki, A., and Uchiyama, A.: Wavelength and NO_x dependent complex refractive index of SOAs generated from the photooxidation of toluene, *Atmos. Chem. Phys.*, 13, 531-545, <https://doi.org/10.5194/acp-13-531-2013>, 2013.
- Nakayama, T., Sato, K., Tsuge, M., Imamura, T., and Matsumi, Y.: Complex refractive index of secondary organic aerosol generated from isoprene/NO_x photooxidation in the presence and absence of SO₂, *J. Geophys. Res.: Atmos.*, 120, 7777-7787, [10.1002/2015jd023522](https://doi.org/10.1002/2015jd023522), 2015.
- 35 Nakayama, T., Sato, K., Imamura, T., and Matsumi, Y.: Effect of Oxidation Process on Complex Refractive Index of Secondary Organic Aerosol Generated from Isoprene, *Environ. Sci. Technol.*, 52, 5, 2566-2574, <https://doi.org/10.1021/acs.est.7b05852>, 2018.



- Ng, N. L., Kroll, J. H., Chan, A. W. H., Chhabra, P. S., Flagan, R. C., and Seinfeld, J. H.: Secondary organic aerosol formation from m-xylene, toluene, and benzene, *Atmos. Chem. Phys.*, 7, 3909-3922, <https://doi.org/10.5194/acp-7-3909-2007>, 2007
- 5 Odum, J. R., Hoffmann, T., Bowman, F., Collins, D., Flagan, R. C., and Seinfeld, J. H.: Gas/particle partitioning and secondary organic aerosol yields, *Environ. Sci. Technol.*, 30, 2580-2585, [10.1021/es950943+](https://doi.org/10.1021/es950943+), 1996.
- Odum, J. R.: The Atmospheric Aerosol-Forming Potential of Whole Gasoline Vapor, *Science*, 276, 96-99, [10.1126/science.276.5309.96](https://doi.org/10.1126/science.276.5309.96), 1997.
- Odum, J. R., Jungkamp, T. P. W., Griffin, R. J., Forstner, H. J. L., Flagan, R. C., and Seinfeld, J. H.: Aromatics, reformulated gasoline, and atmospheric organic aerosol formation, *Environ. Sci. Technol.*, 10 31, 1890-1897, [10.1021/es9605351](https://doi.org/10.1021/es9605351), 1997.
- Peng, C., Wang, W., Li, K., Li, J., Zhou, L., Wang, L., and Ge, M.: The optical properties of limonene secondary organic aerosols: The role of NO₃, OH, and O₃ in the oxidation processes, *J. Geophys. Res.: Atmos.*, 123, 3292-3303, <https://doi.org/10.1002/2017JD028090>, 2018.
- 15 Phillips, S. M., and Smith, G. D.: Light Absorption by Charge Transfer Complexes in Brown Carbon Aerosols, *Environ. Sci. Technol. Lett.*, 1, 382-386, [10.1021/ez500263j](https://doi.org/10.1021/ez500263j), 2014.
- Pope, C. A., Burnett, R. T., Thun, M. J., Calle, E. E., Krewski, D., Ito, K., and Thurston, G. D.: Lung cancer, cardiopulmonary mortality, and long-term exposure to fine particulate air pollution, *Jama - J. Am. Med. Assoc.*, 287, 1132-1141, [10.1001/jama.287.9.1132](https://doi.org/10.1001/jama.287.9.1132), 2002.
- 20 Redmond, H., and Thompson, J. E.: Evaluation of a quantitative structure-property relationship (QSPR) for predicting mid-visible refractive index of secondary organic aerosol (SOA), *Phys. Chem. Chem. Phys.*, 13, 6872-6882, [10.1039/c0cp02270e](https://doi.org/10.1039/c0cp02270e), 2011.
- Santiago, M., Vivanco, M. G., and Stein, A. F.: SO₂ effect on secondary organic aerosol from a mixture of anthropogenic VOCs: experimental and modelled results, *Int. J. Environ. Pollut.*, 50, 25 224-233, [10.1504/IJEP.2012.051195](https://doi.org/10.1504/IJEP.2012.051195), 2012.
- Schulz, M., Textor, C., Kinne, S., Balkanski, Y., Bauer, S., Berntsen, T., Berglen, T., Boucher, O., Dentener, F., Guibert, S., Isaksen, I. S. A., Iversen, T., Koch, D., Kirkevåg, A., Liu, X., Montanaro, V., Myhre, G., Penner, J. E., Pitari, G., Reddy, S., Seland, O., Stier, P., and Takemura, T.: Radiative forcing by aerosols as derived from the AeroCom present-day and pre-industrial simulations, *Atmos. Chem. Phys.*, 6, 5225-5246, <https://doi.org/10.5194/acp-6-5225-2006>, 2006.
- 30 Seinfeld, J. H., and Pandis, S. N.: *Atmospheric chemistry and physics: from air pollution to climate change*, John Wiley & Sons, New York, 2006.
- Shiraiwa, M., Li, Y., Tsimpidi, A. P., Karydis, V. A., Berkemeier, T., Pandis, S. N., Lelieveld, J., Koop, T., and Poschl, U.: Global distribution of particle phase state in atmospheric secondary organic aerosols, 35 *Nat. Commun.*, 8, 15002, [10.1038/ncomms15002](https://doi.org/10.1038/ncomms15002), 2017.



- Staudt, S., Kundu, S., Lehmler, H. J., He, X., Cui, T., Lin, Y. H., Kristensen, K., Glasius, M., Zhang, X., Weber, R. J., Surratt, J. D., and Stone, E. A.: Aromatic organosulfates in atmospheric aerosols: synthesis, characterization, and abundance, *Atmos. Environ.*, 94, 366-373, 10.1016/j.atmosenv.2014.05.049, 2014.
- 5 Sun, Y., Chen, C., Zhang, Y., Xu, W., Zhou, L., Cheng, X., Zheng, H., Ji, D., Li, J., Tang, X., Fu, P., and Wang, Z.: Rapid formation and evolution of an extreme haze episode in Northern China during winter 2015, *Sci. Rep.*, 6, 27151, 10.1038/srep27151, 2016a.
- Sun, Y., Du, W., Fu, P., Wang, Q., Li, J., Ge, X., Zhang, Q., Zhu, C., Ren, L., Xu, W., Zhao, J., Han, T., Worsnop, D. R., and Wang, Z.: Primary and secondary aerosols in Beijing in winter: sources, variations and processes, *Atmos. Chem. Phys.*, 16, 8309-8329, <https://doi.org/10.5194/acp-16-8309-2016>, 2016b.
- 10 Surratt, J. D., Chan, A. W., Eddingsaas, N. C., Chan, M., Loza, C. L., Kwan, A. J., Hersey, S. P., Flagan, R. C., Wennberg, P. O., and Seinfeld, J. H.: Reactive intermediates revealed in secondary organic aerosol formation from isoprene, *Proceedings of the National Academy of Sciences of the United States of America*, 107, 6640-6645, 10.1073/pnas.0911114107, 2010.
- 15 Tao, J., Zhang, L., Cao, J., and Zhang, R.: A review of current knowledge concerning PM_{2.5} chemical composition, aerosol optical properties and their relationships across China, *Atmos. Chem. Phys.*, 17, 9485-9518, <https://doi.org/10.5194/acp-17-9485-2017>, 2017.
- Wang, L., Wang, W., and Ge, M.: Extinction efficiencies of mixed aerosols measured by aerosol cavity ring down spectrometry, *Chin. Sci. Bull.*, 57, 2567-2573, 10.1007/s11434-012-5146-7, 2012.
- 20 Wang, W., Li, K., Zhou, L., Ge, M., Hou, S., Tong, S., Mu, Y., and Jia, L.: Evaluation and application of dual-reactor chamber for studying atmospheric oxidation processes and mechanisms, *Acta Phys.-Chim. Sin.*, 31, 1251-1259, <https://doi.org/10.3866/PKU.WHXB201504161>, 2015.
- Wang, Y., Hu, M., Guo, S., Wang, Y., Zheng, J., Yang, Y., Zhu, W., Tang, R., Li, X., Liu, Y., Le Breton, M., Du, Z., Shang, D., Wu, Y., Wu, Z., Song, Y., Lou, S., Hallquist, M., and Yu, J.: The Secondary Formation of Organosulfates under the Interactions between Biogenic Emissions and Anthropogenic Pollutants in Summer of Beijing, *Atmos. Chem. Phys.*, 19, 2687-2700, <https://doi.org/10.5194/acp-19-2687-2019>, 2019
- 25 Watson, J. G.: Visibility: Science and Regulation, *J. Air Waste Manage. Assoc.*, 52, 628-713, 10.1080/10473289.2002.10470813, 2002.
- 30 Zhang, R., Wang, G., Guo, S., Zamora, M. L., Ying, Q., Lin, Y., Wang, W., Hu, M., and Wang, Y.: Formation of urban fine particulate matter, *Chem. Rev.*, 115, 3803-3855, 10.1021/acs.chemrev.5b00067, 2015.
- Zhao, D., Schmitt, S. H., Wang, M., Acir, I.-H., Tillmann, R., Tan, Z., Novelli, A., Fuchs, H., Pullinen, I., Wegener, R., Rohrer, F., Wildt, J., Kiendler-Scharr, A., Wahner, A., and Mentel, T. F.: Effects of NO_x and SO₂ on the secondary organic aerosol formation from photooxidation of α -pinene and limonene, *Atmos. Chem. Phys.*, 18, 1611-1628, <https://doi.org/10.5194/acp-18-1611-2018>, 2018.
- 35



5 **Table 1. Initial conditions and retrieved average RI of SOA formed under different sets of experiments**

Experiments No.	HC (ppb)	NO (ppb)	NO _x (ppb)	SO ₂ (ppb)	RH (%)	RI average (375 nm)	RI average (532 nm)
D1	182	247	351	<1	<5	1.45	1.412
D2	196	283	425	<1	<5	1.458	1.414
DS1	193	278	425	30	<5	1.37+0.014i	1.348
DS2	160	407	647	50	<5	1.366+0.014i	1.344
W1	170	241	361	<1	>80	1.566+0.022i	1.504
W2	172	235	351	<1	>80	1.562+0.018i	1.508
WS1	165	229	261	35	>80	1.51+0.012i	1.468
WS2	185	257	399	37	>80	1.528+0.01i	1.474

Table 2. Representative identified MS peaks, molecular weight, formula and calculated RI of main products of toluene-derived SOA.

Type	M + H	M + Na	M – H	Molecular Formula	Calculated RI
D		142.94		C ₄ H ₈ O ₅	1.4070
D	137.06			C ₄ H ₉ NO ₂	1.4073
D	162.04			C ₇ H ₁₅ NO ₃	1.4072
D	218.92			C ₁₁ H ₂₂ O ₄	1.4173
D	226.14			C ₇ H ₁₅ NO ₇	1.4124
D			241.23	C ₇ H ₁₄ O ₉	1.4173
D			253.23	C ₉ H ₁₈ O ₈	1.4166
D	261.23			C ₁₄ H ₂₈ O ₄	1.4265
D			269.26	C ₉ H ₁₈ O ₉	1.4175
D			273.04	C ₁₅ H ₃₀ O ₄	1.4264
D	352.24			C ₁₆ H ₃₃ NO ₇	1.4303
D	360.31			C ₁₂ H ₂₅ NO ₁₁	1.4268
D			367.37	C ₁₆ H ₃₂ O ₉	1.4318
D	419.31	441.30		C ₁₅ H ₃₀ O ₁₃	1.4330
DS		113.10		C ₄ H ₁₀ O ₆	1.3595
DS	107.97	130.15		C ₃ H ₉ NO ₃	1.3727
DS	198.11			C ₆ H ₁₅ NO ₆	1.3776



DS	212.15		C ₇ H ₁₆ O ₇	1.3800
DS		233.14	C ₁₂ H ₂₆ O ₄	1.3918
DS		254.24	C ₉ H ₂₁ NO ₇	1.3911
DS		291.14	C ₁₅ H ₃₂ O ₅	1.3950
DS	305.25		C ₉ H ₂₀ O ₁₁	1.3893
DS		337.19	C ₁₆ H ₃₅ O ₇	1.3997
DS		346.02	C ₁₁ H ₂₅ NO ₁₁	1.3972
DS		353.18	C ₁₆ H ₃₄ O ₈	1.4004
DS		381.21	C ₁₉ H ₃₂ O ₈	1.4032
DS		397.20	C ₁₈ H ₃₈ O ₉	1.4032
DS	455.31		C ₂₂ H ₄₆ O ₉	1.4085
DS	475.38		C ₂₀ H ₄₂ O ₁₂	1.4066
DS		514.36	C ₂₃ H ₄₉ NO ₁₁	1.4122
W		223.02	C ₁₂ H ₁₆ O ₄	1.5459
W	318.24		C ₁₄ H ₂₇ NO ₇	1.5227
W		323.23	C ₁₁ H ₁₆ O ₁₁	1.5230
W	346.33		C ₁₆ H ₂₇ NO ₇	1.5258
W		422.18	C ₁₇ H ₂₉ NO ₁₁	1.5313
W		459.28	C ₂₃ H ₄₀ O ₉	1.5364
W		467.04	C ₁₉ H ₃₂ O ₁₃	1.5334
W	509.25		C ₂₃ H ₄₀ O ₁₂	1.5374
W		523.22	C ₂₃ H ₄₀ O ₁₃	1.5380
W		541.05	C ₂₂ H ₃₈ O ₁₅	1.5366
W	559.50		C ₂₂ H ₃₈ O ₁₆	1.5382
W	583.51		C ₂₆ H ₄₆ O ₁₄	1.5423
W	615.15		C ₂₆ H ₄₆ O ₁₆	1.5432
W	641.60		C ₂₉ H ₅₂ O ₁₅	1.5465
W	642.60		C ₂₈ H ₅₁ NO ₁₅	1.5461
WS	203.05		C ₉ H ₁₄ O ₅	1.4793
WS		217.04	C ₉ H ₁₄ O ₆	1.4762
WS		271.09	C ₁₄ H ₂₄ O ₅	1.4904
WS		279.04	C ₁₀ H ₁₆ O ₉	1.4875
WS		301.04	C ₁₅ H ₂₆ O ₆	1.4918
WS	315.16		C ₁₇ H ₃₀ O ₅	1.4950
WS		317.06	C ₁₅ H ₂₆ O ₇	1.4926
WS		331.06	C ₁₆ H ₂₈ O ₇	1.4941
WS		341.09	C ₁₁ H ₁₈ O ₁₂	1.4878
WS	365.11		C ₁₆ H ₂₈ O ₉	1.4974
WS		379.06	C ₁₆ H ₂₈ O ₁₀	1.4954



WS	409.29		$C_{18}H_{32}O_{10}$	1.4974
WS		409.08	$C_{17}H_{30}O_{11}$	1.4974
WS		415.02	$C_{14}H_{24}O_{14}$	1.4945
WS		429.03	$C_{15}H_{26}O_{14}$	1.4945
WS		461.04	$C_{23}H_{42}O_9$	1.5036
WS		483.04	$C_{20}H_{36}O_{13}$	1.5032
WS	522.60		$C_{25}H_{47}NO_{10}$	1.5081
WS	550.70		$C_{27}H_{51}NO_{10}$	1.5109
WS		580.98	$C_{27}H_{50}O_{13}$	1.5126
WS		597.21	$C_{27}H_{50}O_{14}$	1.5125

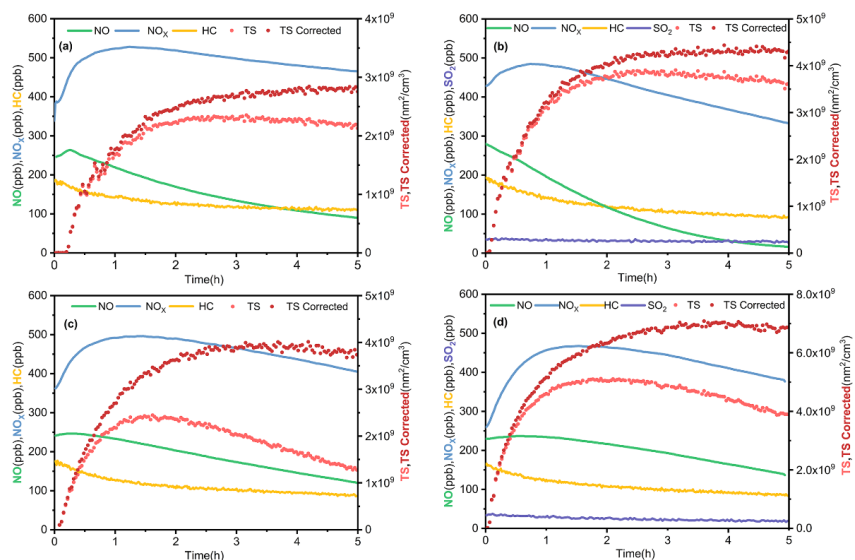


Figure 1. Reaction profiles of photooxidation of toluene under four different conditions: (a) D1 (dry condition), (b) DS1 (dry condition with SO_2), (c) W1 (wet condition), (d) WS1 (wet condition with SO_2); see Table 1 for details. The concentrations of gas species are shown in the left axis, while the concentrations of particles are shown in the right axis.

10

15

20

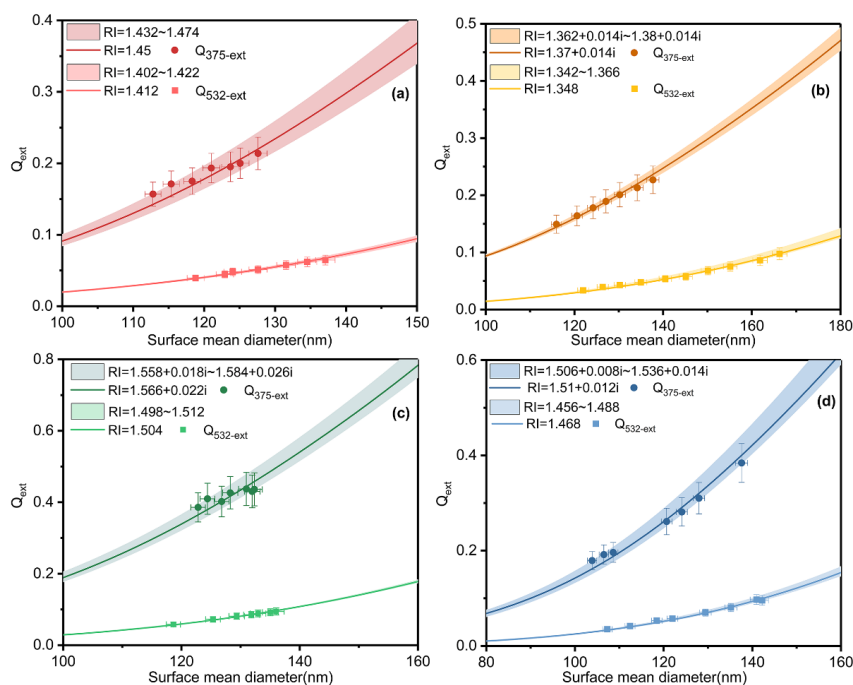


Figure 2. Dependence of the extinction efficiencies of SOA on the surface mean diameter by four different conditions at (a) D1, (b) DS1, (c) W1, (d) WS1. The lines are results retrieved from average RI, while the shadows are range of retrieved RI.

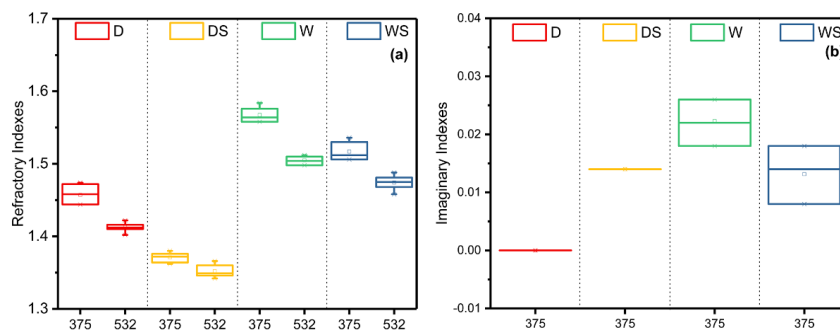


Figure 3. Difference of the values of (a) refractive indexes and (b) imaginary indexes for toluene-derived SOA under four different conditions at 375 nm and 532 nm. The values of k are zero at 532 nm and not shown in the figure.

5

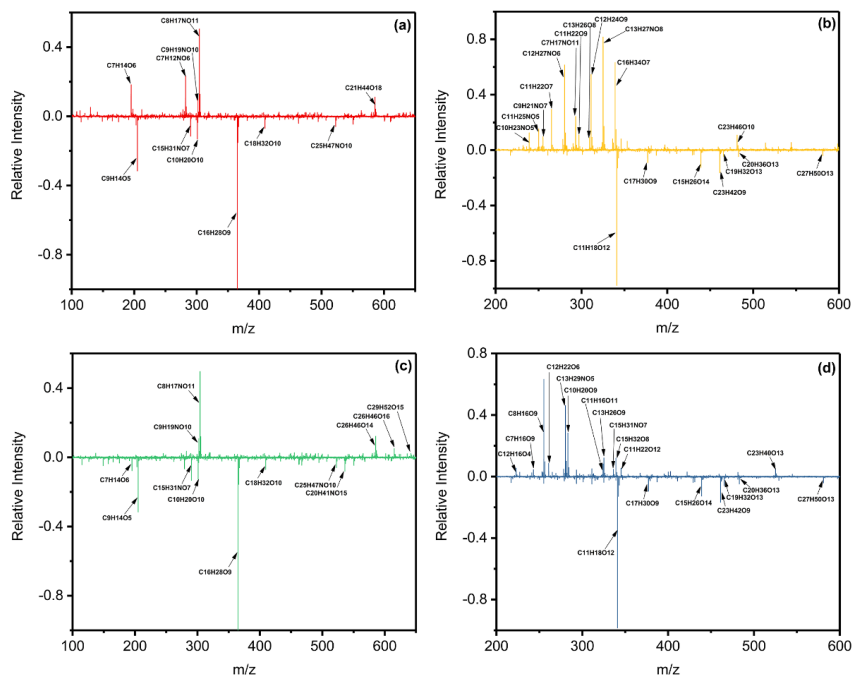


Figure 4. MS difference between condition DS and WS in (a) positive, (b) negative mode, between condition W and WS in (c) positive and (d) negative mode. The Y axis is the subtraction of relative intensity (indicated by the peak intensity relative to the strongest peak intensity) between condition DS or W and WS. Products whose relative intensities above zero are in a higher concentration under condition DS or W while those below zero are on the contrary.

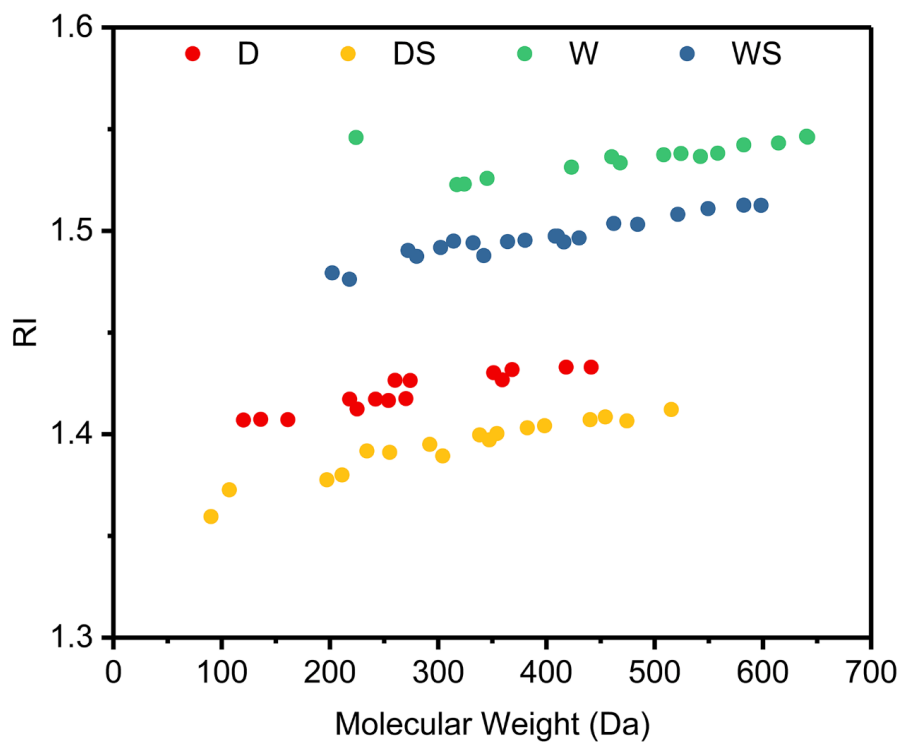


Figure 5. The unique molecular weight and calculated RI under four conditions.

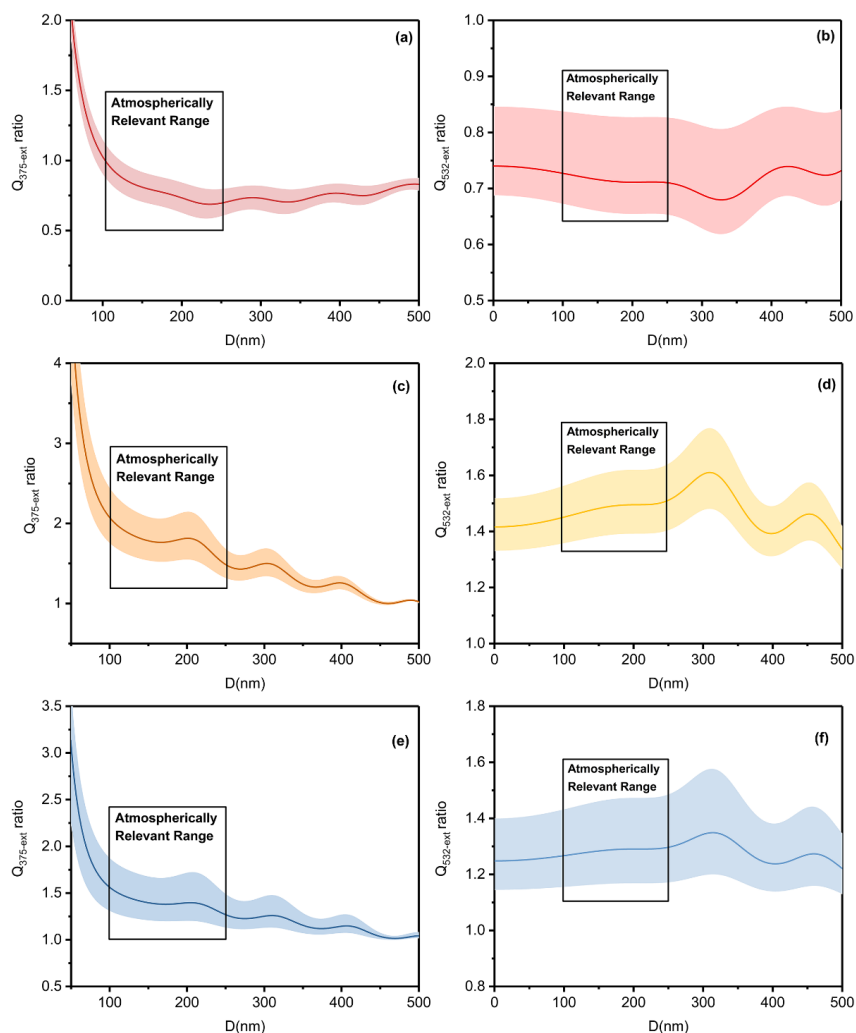


Figure 6. The ratio of light extinction efficiency of toluene secondary organic aerosol of condition DS to condition D at (a) 375 nm, (b) 532 nm, of condition W to condition D at (c) 375nm, (d) at 532nm, of condition WS to condition D at (e) 375 nm, (f) 532 nm. The lines are the average values, the shaded areas are 5 uncertainties and the box areas represent atmospherically relevant range.